A Low-Cost Flash Photographic System for Visualization of Droplets in Drop-on-Demand Inkjet

Huicong Jiang, Brett Andrew Merritt, and Hua Tan

School of Engineering and Computer Science, Washington State University Vancouver, 14204 NE Salmon Creek Ave,
Vancouver, WA 98686, USA
E-mail: hua.tan@wsu.edu

Abstract. *Flash photography has been widely used to study the droplet dynamics in drop-on-demand (DoD) inkjet due to its distinct advantages in cost and image quality. However, the whole setup, typically comprising the mounting platform, flash light source, inkjet system, CCD camera, magnification lens and pulse generator, still costs tens of thousands of dollars. To reduce the cost of visualization for DoD inkjet droplets, we proposed to replace the expensive professional pulse generator with a low-cost microcontroller board in the flash photographic system. The temporal accuracy of the microcontroller was measured by an oscilloscope. The microcontroller's temporal stability was compared with a professional pulse generator by tracking a large number of droplet positions. To validate the effectiveness of the whole setup, the droplet ejection and the droplet impact on a silicon wafer were quantitatively analyzed and compared with theoretical predictions. Finally, sample images of droplet ejected from a commercial inkjet cartridge were presented to show the flexibility of the system.*
ⓒ *2018 Society for Imaging Science and Technology.*
[DOI: 10.2352/J.ImagingSci.Technol.2018.62.6.060502]

1. INTRODUCTION

Drop-on-demand (DoD) inkjets, often associated with text and graphic printers, now see diverse applications ranging from the manufacturing of electronics [1] to tasks such as improving detection of target molecules [2]. As novel applications of DoD inkjet are emerging, there is growing demand to fundamentally understand the droplet dynamics (e.g., droplet formation, droplet–substrate interaction [3]) in these applications. Visualization is the most direct and convincible way to study droplet dynamics. However, observing the droplets in DoD inkjet is a demanding task, because the fast speed (meters per second) of ejected microscopic droplets (tens of micrometers) requires a very short exposure time [4]. To capture the images of droplet evolution in inkjet process, one can resort to an ultra-high-speed camera with exposure time less than 0.5 μs and frame rate exceeding 1 MHz to directly record single events as they occur. Nevertheless, these cameras are often very expensive and have low spatial resolution at very high frame rate [5]. Alternatively, flash photography can be used to avoid these drawbacks due to the high repeatability of fluid phenomena in inkjet process. Instead of pushing cameras to

the extreme, it tries to reduce the flash time of the light source which is much easier than improving the shutter speed of a camera and can be compatible with most of the cameras. Although only one image can be taken from an event through this method, by leveraging the high reproducibility of the DoD inkjet and delaying the flash, a sequence of images freezing different moments can be acquired from a series of identical events and then yields a video recording the whole process. It is noteworthy that flash photography should be distinguished from the stroboscopic imaging [6]. The latter flashes many times per frame in synchronization with the droplet generation. In contrast, the former just expose the camera once in a frame. Due to the timing jitter and the slight difference between each ejection, droplets recorded stroboscopically are usually blurrier than that produced by the flash photography.

Over the years, flash photography has become a standard method to investigate the droplet dynamics in DoD inkjet due to its distinct advantages in cost and image quality. Dong et al. [7, 8] present a flash photographic setup with high spatial and temporal resolution which enables quantitative analysis. By using a copper-vapor pulsed laser as the light source with flash duration of 25 ns and power of 2 mJ, they successfully acquired sharp images from droplet formation and impact, and quantified the time-dependent positions of leading and trailing edges of droplets. To promote quantitative analysis, Hutchings et al. [9, 10] pioneered an image processing program, PEJET, which can automatically find the droplet edge and calculate droplet volume. As examples, tail-width fluctuations, lateral deflections, and satellite velocities were quantitatively analyzed. After these two remarkable studies, flash photography together with the computer-aided optical measurement techniques [11–16] gained wide popularity in a range of research on droplet dynamics in DoD inkjet. Droplet spreading on smooth solid surface [17–19], various influence factors for droplet formation (such as voltage waveforms [20, 21] and fluid physical properties [22, 23]) and the non-Newtonian fluid phenomena in polymer solution inkjet [23, 24] were all systematically studied. Recently, the most notable advance in flash photography can be the illumination by laser-induced fluorescence (iLIF) technique raised by van der Bos et al. [25] which reduced the flash duration to 7 ns and increased the power to 100 mJ. This extremely short and powerful illumination improved the image quality to a level that even
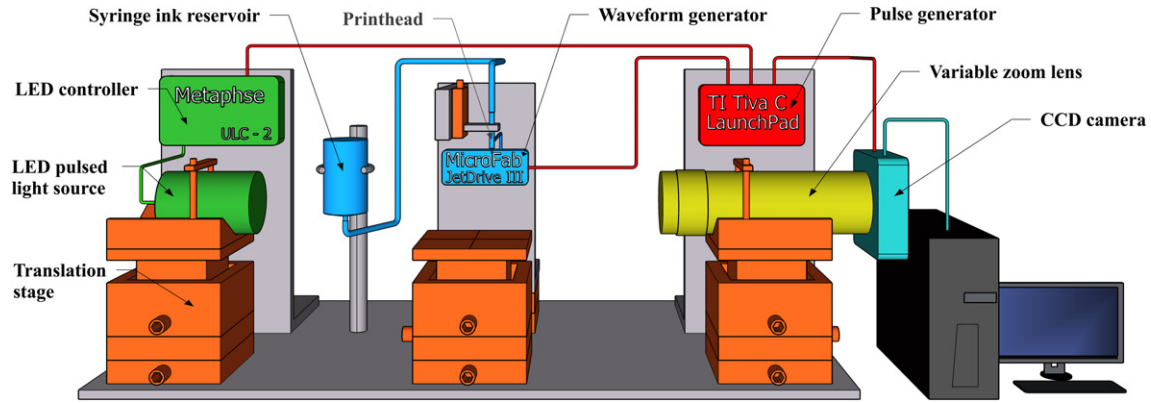
Figure 1. Schematic of flash photographic setup.

the instantaneous velocity profile inside a droplet can be calculated with high accuracy [16].

Although the apparatus models and their capacities used in these research are different, all of these flash photographic systems invariably consist of six components, i.e., mounting platform, flash light source, inkjet system, CCD camera, magnification lens and pulse generator. Building a whole system from scratch can cost tens of thousands of dollars which, although much cheaper than the real-time high-speed camera, is still a big budget for new labs. Among these six components, a professional pulse generator usually costs more than three thousands US dollars, which can take 10–20% of the total cost of the DoD imaging system. Therefore, to further reduce the cost of visualization for DoD inkjet droplets, in this study we used a low-cost microcontroller board (typical cost is less than a hundred US dollars) as the pulse generator in a flash photographic system. The temporal accuracy of the microcontroller board was first measured by an oscilloscope and then the temporal stability was compared with a professional pulse generator by tracking a large number of droplet positions. To validate the effectiveness of the whole setup, droplet ejection and impact were quantitatively analyzed and compared with theoretical predictions. In the end, images of droplet ejected from a commercial inkjet cartridge were presented to show the flexibility of the system.

2. EXPERIMENTAL SETUP AND METHOD

The flash photographic setup used in this work is schematically shown in Figure 1. Images were acquired by a 640×480 pixels monochrome CCD camera (340M-GE Thorlabs, NY, USA) with pixel size of 7.4×7.4 μm². The magnification lens consisting of a $12\times$ variable zoom lens (MVL12X12Z, Thorlabs, features $0.58 \times -7\times$ magnification), a $2\times$ magnifying lens attachment (MVL12X20L, Thorlabs) and a $2\times$ magnifying extension tube (MVL20A, Thorlabs) provided an overall magnification from $2.32\times$ to $28\times$ for the camera. A pulsed LED light source (HiSLED-1003, Metaphase Technologies, PA, USA) with a minimum flash duration of 100 ns was controlled by a

universal LED controller (ULC-2 Metaphase Technologies) to back-illuminate the inkjet droplet.

To validate the compatibility of the camera, lens and light source, Rayleigh criterion and spatial Nyquist criterion are applied [4, 25]. The Rayleigh criterion features the minimum resolvable feature size (spatial resolution) of a lens under a specific light source and the spatial Nyquist criterion can calculate the required magnification for a specific spatial resolution and pixel size. Thus, if the magnification range of the lens can satisfy the required magnification, the aforementioned three components are well fitted, otherwise the image is under-sampled [26]. Rayleigh criterion is shown in Eq. (1) in which the d_f, λ and *NA* are the spatial resolution, light wavelength and numerical aperture, respectively.

$$d_f = 1.22 \frac{\lambda}{2NA}. \tag{1}$$

Because the numerical aperture of the lens assembly ranges from 0.038 to 0.202, applying this range into Rayleigh criterion and assuming the average wavelength of LED light as 550 nm yields a spatial resolution spectrum from 8.82 μm to 1.66 μm. Spatial Nyquist criterion is shown in Eq. (2) in which the *M* and d_p are required magnification and pixel size, respectively.

$$M > \frac{2d_p}{d_f}. \tag{2}$$

By substituting the nominal pixel size of 7.4 μm and the calculated spatial resolution into Eq. (2), we can get a minimum required magnification of $1.68\times$ at the low end and $8.92\times$ at the high end, both of which are satisfied by the lens assembly. Therefore, our combination of the camera, lens and light source are appropriate.

The inkjet system comprises three parts and a software, all of which are purchased from Microfab Technologies (TX, USA). Droplets of deionized water were produced by a single nozzle piezoelectric printhead (MJ-AB-030) with a nozzle diameter of 30 μm. To maintain a constant negative water head at the nozzle, a syringe ink reservoir (100 ml) with large cross section was connected to the printhead through a PVT tube (1 mm internal diameter) and the liquid level
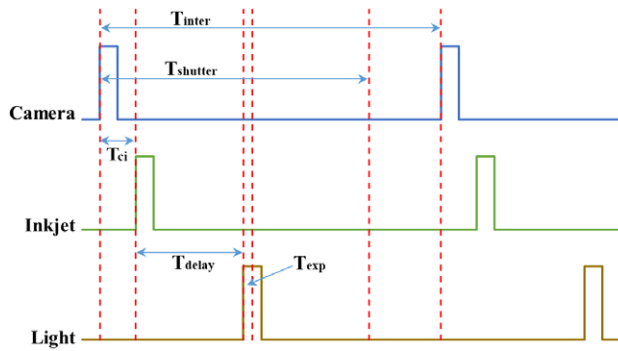
Figure 2. Timing diagram.

was positioned slightly lower than the nozzle. Due to the tiny volume of the droplets, the small change of liquid level resulted from hundreds of jets can be neglected. A waveform generator (JetDrive III) which can be edited through a waveform design software (JetServer) was used to deliver the driving waveform for the printhead.

In order to reduce the cost of the setup, a low-cost ($13) microcontroller board, Texas Instruments Tiva C LaunchPad TM4C123G (referred to as LaunchPad hereinafter), was adopted to coordinate the transistor–transistor logical (TTL) trigger signals delivered to the inkjet system, CCD camera, and LED light source. The technical details of the LaunchPad including software, drivers, and documentation can be found in Ref. [27]. The timing diagram is shown in Figure 2. Note that all the devices were edge triggered, thus the dwell time of the trigger signal does not necessarily represent the duration of an event, such as the flash and the shutter. The following settings were applied to all the experiments reported below. Camera was triggered first and followed by the Inkjet with a fixed delay T_{ci} of 20 μs. The shutter duration $T_{shutter}$ was set to 1 ms which allows for an adjustment of the delay time between inkjet and light source T_{delay} to observe all the droplet formation processes within a standard stand-off distance of 1 mm (assuming the minimum speed of droplet is 1 m s^{-1}). The interframe time T_{inter} is determined by the speed of the camera which has a highest frame rate of 200 Hz. Thus, the minimum interframe time is 5 ms. Although the LED controller can vary flash duration T_{exp} from 100 ns to 300 ns, the minimum value of 100 ns was used to reduce the motion blur, which also provided good image brightness even at high magnification. For uniformity, all the trigger polarities were set as high level with high voltage of 3.3 v, low voltage of 0 v and dwell time of 10 μs.

To make the system more flexible and accommodate different functions, the camera–lens assembly, printhead, light source and substrate sample were all positioned on X–Y–Z linear translation stages (Newport, CA, USA) which have a sensitivity of 1 μm. The whole setup was assembled on top of a small optical table (Nexus B1236F, Thorlabs) to minimize the deflection and vibration of the working surface.

Different from the microscope objective, the variable zoom lens cannot provide an accurate magnification factor. Therefore, for each set of experiments, the length scale was determined by taking an image of a microscope calibration slide (10 μm fine scale) at the same magnification as the droplet images. Because it was observed that adjusting the built-in focus to view the slide (thereby shifting the focus plane relative to the lens) led to slightly different length scale even at the same magnification, to avoid inconsistencies in length measurements, translation of the entire camera–lens assembly was used for focus adjustments after calibration.

3. TEMPORAL ACCURACY AND STABILITY

Temporal accuracy and stability are the most important properties for a pulse generator in flash photography, since any slight timing deviation and jitter will result in variations of droplet shape and position. For a specific microcontroller board, these two critical properties are determined by the library functions provided by the microcontroller. Different function libraries of microcontroller appear to achieve the same function, however their process in the microcontroller is very different, hence resulting in different temporal properties. For example, in Energia, the LaunchPad associated integrated development environment (IDE), the library function delaymicrosecond (1000) and delay(1) combined with the digitalwrite() both can command LaunchPad to generate a 1 ms pulse. However, for single high level pulse, the delaymicrosecond(1000) in reality produces an extra pulse width of 3.510 μs without jitter, whereas the delay(1) has a smaller extra time of 1.750 μs with a jitter in the range from +0.600 μs to −0.176 μs. Furthermore, the pulse width deviation and jitter even vary from pulse to pulse in a burst of pulses with the same function. As a result, the assessment of temporal accuracy and stability of the LaunchPad for a specific time function needs to be first conducted to understand performance of the setup. The code used in our experiment is shown in the Appendix.

3.1 Temporal Accuracy

The temporal accuracy of a pulse generator usually includes three aspects: the pulse width, delay time and period (frequency). However, only the accuracy of the delay time between the inkjet signal and the flash signal can directly affect the images of inkjet droplets. Therefore, this delay time was measured by an oscilloscope (Tektronix DPO 2024B) with a precision of 1 ns and the results were shown in Table I.

It is evident in Table I that the delay time deviation is very stable when the nominal delay is less than 1010 μs with only negligible 5 ns increase from 2.850 μs at 11 μs nominal delay to 2.855 μs at 910 μs nominal delay, representing the accurate time increase within 1010 μs. However, when the nominal delay is above the 1010 μs, the extra time increased significantly by 1.905 μs–4.760 μs and continues to increase with every additional 1000 μs nominal delay. Although several microseconds deviation is a considerable time scale in terms of inkjet droplet dynamics, it does not significantly affect the quantitative analysis of imaged inkjet droplets. The reason is that the analysis of captured images of inkjet process requires a constant and stable delay time between pluses rather than an exact delay time specified by the user.

Table I. Measured delay time between inkjet signal and flash signal.

Nominal delay (μs)	Measured delay (μs)	Extra time (μs)
11	13.850	2.850
110	112.850	2.850
210	212.851	2.851
310	312.851	2.851
410	412.852	2.852
510	512.852	2.852
610	612.853	2.853
710	712.853	2.853
810	812.854	2.854
910	912.855	2.855
1010	1013.510	3.510
2010	2015.160	5.160
3010	2016.820	6.820

Figure 3. Droplet edge (red line) detection and droplet position measurement.

Therefore, if the delay range is within 1010 μs, the accuracy of the time variation analysis can be guaranteed. Most of the physical events of inkjet droplet take place within 1 ms after the trigger of inkjet and hence using the LaunchPad as a replacement of the pulse generator in the imaging system is acceptable in terms of delay time in most cases.

3.2 *Temporal Stability*

Although the temporal jitter range can be measured by the oscilloscope (Tektronix DPO 2024B), it is unable to record the time variation of the jitter which is more important for the assessment of temporal stability. Therefore, an indirect way is proposed to evaluate the temporal stability. By tracking a large number of droplet positions at a given jetting condition (speed, shape and position) and comparing standard deviation with that of a reference device, we can evaluate the temporal stability of the LaunchPad. The reference device we used is a widely implemented professional pulse generator (model 505, Berkeley Nucleonics, CA, USA, referred to as BNC-505 hereinafter). The cost of BNC-505 is around 3000 US dollars. Both the BNC-505 and LaunchPad were applied to collect images of 500 droplets produced in sequence at frequency of 10 Hz. To avoid the first droplet problem, the first 50 droplets were skipped over, and recording was started from the 51st ejection. At the time of image capture, the droplet velocity was 14.1 m s^{-1}, a relatively high speed for inkjet droplets intended to exaggerate variations in droplet position. The droplet position was defined as the distance between the crop line and the droplet leading edge which was located using a Canny [28, 29] edge-detection algorithm in MATLAB. It is well known that the uneven light intensity distribution in captured images and variations of the intensity of the light source often result in the measurement errors using the edge-detection method based image analysis [14, 30, 31], hence we use the two-pass edge-detection method proposed by Van der Bos et al. [16] to minimize these errors. Figure 3 shows a typical droplet edge detection and position measurement process.
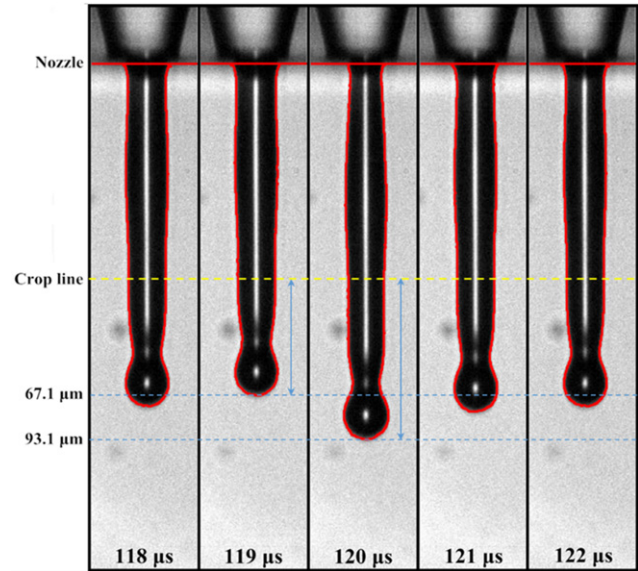
Figure 4(b) shows the position of droplets signaled by the BNC-505 which, for all 500 droplets, has a statistic value of 67.7 $\pm$ 4.41 μm (mean value $\pm$ standard deviation). Knowing the average droplet velocity to be 14.1 m s^{-1}, the standard deviation of timing jitter can be estimated to be around 0.3 μs. Note that this jitter is the cumulative effect of the whole system including the BNC-505, inkjet system, light source and CCD camera. Figure 5(b) shows the standard deviation of the droplet position as calculated from increasingly larger sample size. The first point represents the variation of first 10 position measurements, the second represents the first 20, and so on with the final point calculated based on all 500 measurements. Given the regularity of the variation, the calculated standard deviation rapidly converges from around 4.6 μm to 4.1 μm, a reduction of nearly 10%, as the sample size increases from 10 frames to around 30 frames.

The position of droplets produced using the LaunchPad is plotted in Fig. 4(a). For all 500 droplets in comparison with that of the BNC-505, and the standard deviation increases by 0.5 μm reaching 4.6 μm. By dividing these increments by the droplet velocity, we can find that the LaunchPad only has a 0.03 μs higher fluctuation than the BNC-505 which are negligible in inkjet droplet dynamics. Thus, the temporal accuracy and stability of the LaunchPad is pretty reasonable and its results are generally comparable with the BNC-505. One interesting aspect of the LaunchPad's performance is that it is affected by what appears to be periodic spikes in latency. These are seen as the dramatically increased position around frames 125 (shown in Fig. 3) and 340. The positional difference between these peaks and the average position is around 18 μm which corresponds to approximately 1.3 μs jitter in timing. One consequence of this is that the standard deviation converges very slowly with increasing sample size which can be seen in Fig. 4(a).
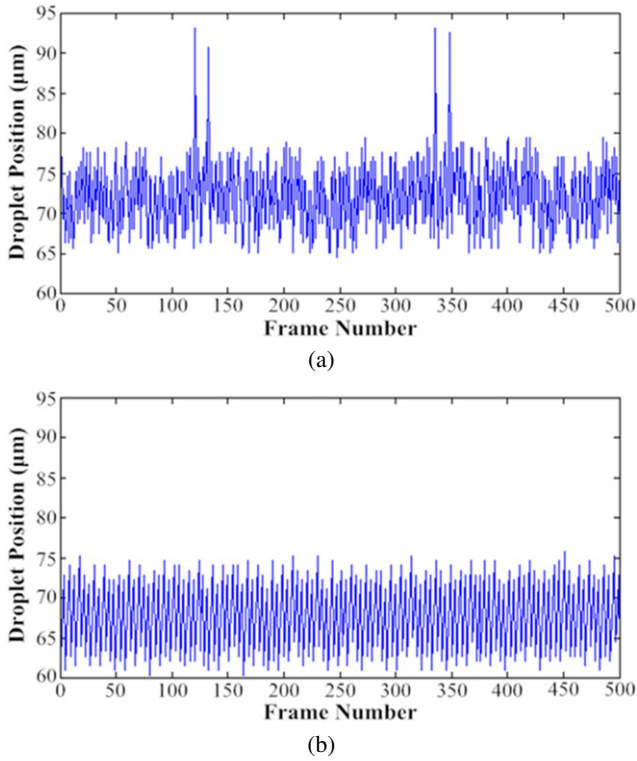
(a)

(b)

Figure 4. Variations of droplet position: (a) LaunchPad, (b) BNC-505.

(a)

(b)

Figure 5. Standard deviation of droplet position with increasingly larger sample size: (a) LaunchPad, (b) BNC-505.

4. EXAMPLES

To validate the effectiveness of the whole setup, two common phenomena in inkjet droplets were quantitatively analyzed and compared with the theoretical predictions. The first example is the droplet oscillation after breakup in which oscillation period and damping time were studied. The second example is a droplet impacting on a smooth silicon wafer in which the spreading and contraction were analyzed. Finally, images of droplet ejected from a commercial inkjet cartridge were presented to show the flexibility of the system.

4.1 *Droplet Ejection*

When a droplet is ejected from the inkjet printhead, a liquid ligament is initially emerging from the nozzle. After a short period, the growing ligament will pinch off from the nozzle to form a free-flying thin filament that will contract due to surface tension. Depending on the fluid properties, the filament either forms a single droplet or breaks up into multiple droplets. In either case, the droplets will oscillate many times before reaching the stable state. The oscillation of a free droplet has been studied extensively in the past. Two characteristic times (i.e., capillary time τ_{cap} and viscous time τ_{visc}) can predict the order of magnitude of the oscillation period and the damping time. The expressions of these two characteristic times are presented in Eqs. (3) and (4)

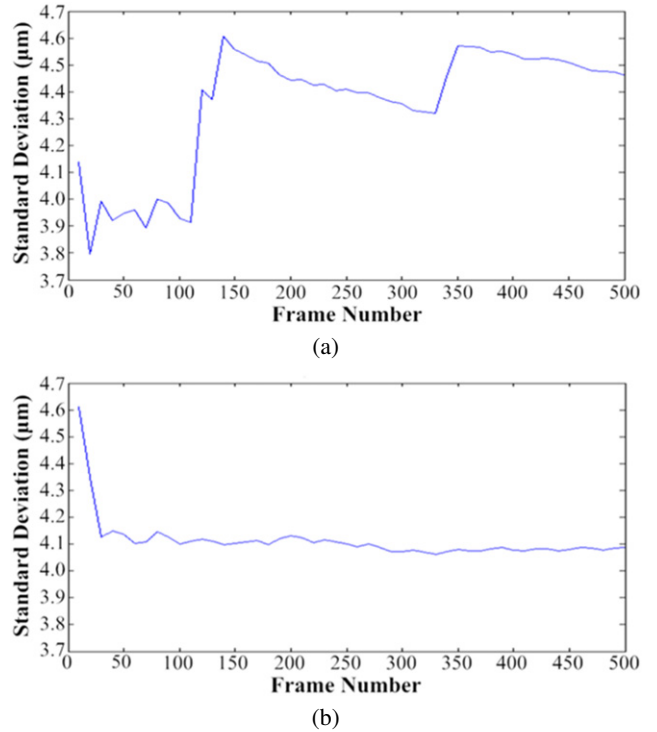$$\tau_{\text{cap}} = \sqrt{\frac{\rho D^3}{\sigma}} \tag{3}$$

$$\tau_{\text{visc}} = \frac{\rho D^2}{\mu} \tag{4}$$

where ρ, σ, μ and D are density, surface tension, viscosity and droplet diameter, respectively. The deionized water is used in the experiment with the properties at room temperature $\rho = 998.21 \text{ kg m}^{-3}$, $\sigma = 72.86 \text{ mN m}^{-1}$, $\mu = 1.0016 \text{ cP}$.

Figure 6(a) shows the droplet-ejection process captured by our flash photographic system. Images were captured with an interval of 1 μs in experiment, whereas the interframe time shown in Fig. 6(a) is 5 μs. We can clearly see that as the ligament is emerging from the orifice under the pressure pulse, a blob is growing at the end of the ligament due to surface tension. When the ligament pinches off from the nozzle at 24 μs, it consists of a near-spherical massive head, with the diameter nearly identical to the nozzle diameter (i.e., 30 μm), followed by a tapering filament in the tail. Next, the ligament breaks up into a large primary head droplet and a thin filament that eventually contracts into a single smaller droplet (which is often referred to as the satellite droplet). The length L and diameter D of the filament are 45 μm and 8 μm, respectively, and the Ohnesorge number $Oh = \mu/(\rho\sigma D)^{1/2} = 4.17 \times 10^{-2}$. According to the experimental study on filament breakup in DOD inkjet printing done by Hoath et al. [32], the liquid filament with an aspect ratio $\alpha = L/D = 5.625$ and $Oh = 4.17 \times 10^{-2}$ will collapse into one single droplet without the breakup, which is in agreement with our experiment.

As the thin filament collapses into the satellite droplet, it undergoes a series of oscillations with diminishing amplitude due to surface tension and viscous force. The oscillation of
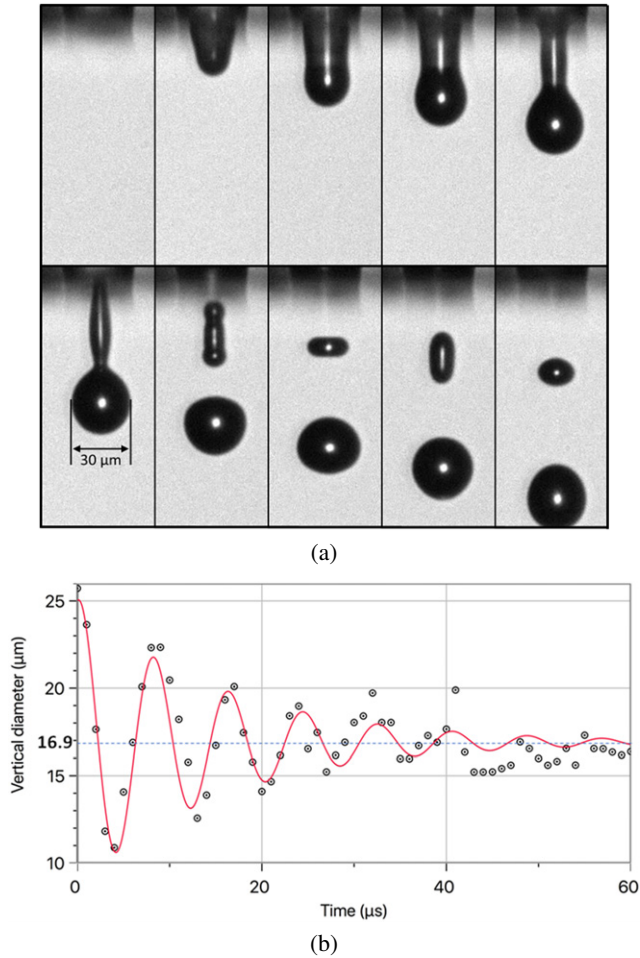
(a)

(b)

Figure 6. (a) Formation of an oscillating satellite droplet during droplet-ejection process (interframe time of 5 µs). (b) Variation of the vertical diameter of the oscillating satellite droplet with time interval of 1 µs. The solid line is the damped harmonic oscillation fitting curve for the scattered experimental data.

the satellite droplet can be demonstrated by the plot of time history of vertical diameter of the satellite droplet as shown in Fig. 6(b). It is clear from the figure that the oscillation of the droplet diameter is gradually diminishing due to the viscous damping effect. A classical damped harmonic oscillation can be used to fit the scattered experimental data as following

$$D_v(t) = D_{eq} + D_{amp}e^{-t/\tau_{damp}} \sin[2\pi(t - \tau_1)/\tau_{osc}] \quad (5)$$

where D_v, D_{eq}, D_{amp}, τ_{damp}, τ_1 and τ_{osc} are vertical diameter, equilibrium diameter, oscillation amplitude, damping time, lagging time and oscillation period, respectively. By using the software package Logger Pro 3, fitting curve (red line) can be easily found and the parameters in Eq. (5) are identified as $D_{eq} = 16.90$ µm, $D_{amp} = 8.25$ µm, $\tau_{damp} = 15.75$ µs, $\tau_1 = 1.79$ µs and $\tau_{osc} = 8.10$ µs. Substituting the water properties at the room temperature and the equilibrium diameter $D = 16.90$ µm into Eqs. (3) and (4) yields $\tau_{cap} = 8.13$ µs and $\tau_{visc} = 284.64$ µs. The capillary time τ_{cap} agrees well with the experimentally measured oscillation period τ_{osc}. However, the viscous time is much longer than

the damping time. This large discrepancy can be attributed to the air stress exerted to the droplet which dissipates extra amount of energy besides the viscosity. The viscous time predicted by Eq. (4) is derived with the assumption that the droplet is only under the interaction between viscosity and surface tension. We need to point out that the discrepancy between the predictions by the harmonic damping oscillation equation and experimental measurements can be caused by the fact that we neglect high order terms for large amplitude oscillation in our analysis [33].

4.2 Droplet Impact On a Solid Surface

In this experiment, a water droplet of diameter $D = 39.30$ µm impacting on a smooth wafer surface at a speed of $u = 2.49$ m s^{-1} was captured by our imaging system. The evolution of the droplet profile is shown in Figure 7(a). The time history of the droplet height is shown in Fig. 7(b). It is clear that after the initial phase of the impact on the solid surface, the droplet also experiences a similar damped oscillation as the oscillating droplet in the flight discussed in section 4.1. The time variation of the height of the droplet h also follows the harmonic equation as following

$$h_v(t) = h_{eq} + h_{amp}e^{-t/\tau_{damp}} \sin[2\pi(t - \tau_1)/\tau_{osc}] \quad (6)$$

where h_v, h_{eq}, and h_{amp} are instantaneous height, equilibrium height and oscillation amplitude, respectively. The fitting curve is found based on the discrete data from experiment. The parameters in Eq. (6) are identified as $h_{eq} = 23.44$ µm, $h_{amp} = 4.23$ µm, $\tau_{damp} = 51.68$ µs, $\tau_1 = -5.20$ µs and $\tau_{osc} = 20.11$ µs. With the water properties at room temperature and the droplet diameter, we calculate the capillary time $\tau_{cap} = 28.80$ µs and viscous time $\tau_{visc} = 1538.94$ µs using Eqs. (3) and (4), respectively. The oscillation period τ_{osc} obtained from the curve-fitting of Eq. (6) using experimental data is close to the theoretical capillary time τ_{cap}. The damping time is 0.03 of the viscous time which is consistent with Lim's experimental result ($0.02\tau_{vis}$) [34]. In this example the Weber number $We = \rho u^2 D/\sigma = 3.34$ and Reynolds number $Re = \rho uD/\mu = 97.53$, so the dynamics of the droplet spreading falls into the inertia-driven impact regime according to Schiaffino's classification [35]. The time evolution of the contact radius is plotted in Fig. 7(c). It can be seen that after the droplet spreads to the maximum extension the contact line is nearly pinned despite the oscillation of the droplet. The time history of the spreading factor $\beta = D_{spread}/D$ in the initial spreading phase is plotted in Fig. 7(d). We find that the relation of the spreading factor β and dimensionless time $\tau = t/\tau_{osc}$ can be expressed by a power function as $\beta = 12.6\tau^{0.27}$ (i.e., solid line in Fig. 7(d)). The maximum spreading factor $\beta_{max} = 1.32$ measured from the experiment is in a good agreement with Bayer's theoretical prediction [36] $\beta_{max} = 0.72(ReWe^{0.5})^{0.14} = 1.49$.

4.3 Commercial Inkjet Droplet Visualization

In this test, a commercial inkjet cartridge (Hewlett Packard, C6602A) is used to demonstrate the effectiveness of the proposed imaging system. In contrast to the inkjet system
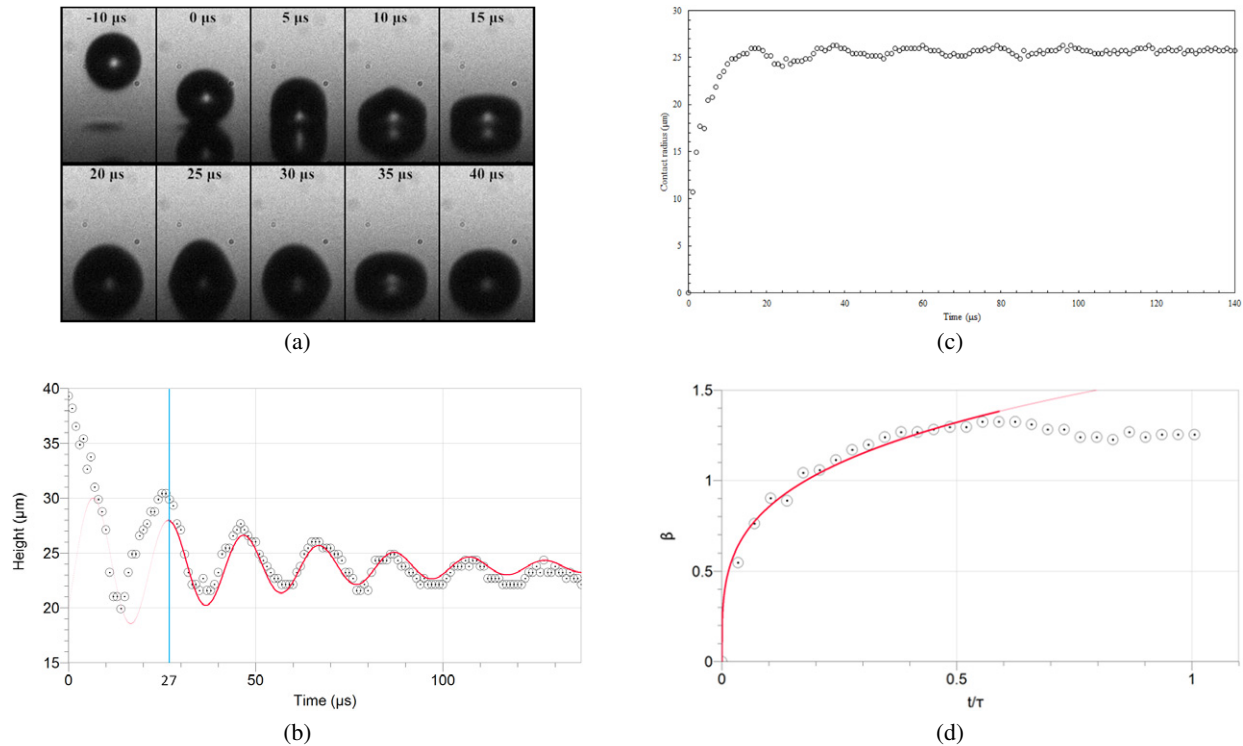
(a)

(c)

(b)

(d)

Figure 7. (a) The evolution of the droplet profile during droplet impact on the silicon wafer surface, (b) the time history of droplet height after the droplet impact. The solid line is the damped harmonic oscillation fitting curve for the scattered experimental data. (c) Time history of the contact radius. (d) The spreading factor β versus dimensionless time τ follows the power law as $\beta \sim \tau^{0.27}$.

described above, we do not have a tight control over individual inkjet firing events for this commercial printhead. Droplets ejected from HP's printhead can only have a fixed frequency of 1152 Hz which is too high for the camera (maximum frame rate of 200 Hz) to match. Thus, the frequency of the trigger signals delivered to the camera and light source were set as an integer multiple of the droplet frequency. By fine tuning the frequency to 48 Hz, it was possible to capture images of every 24 droplets such that they appeared in the same position each time as shown in Figure 8. Therefore, it was possible to synchronize two entirely separate systems. It is clear that our proposed flash photography can successfully capture the dynamics of inkjet droplets with reasonable accuracy.

5. CONCLUSION

By replacing a professional pulse generator with a much lower cost microcontroller in a flash photographic system, the cost of visualization for droplets in DoD inkjet can be greatly reduced by around 3000 US dollars in our study. The temporal accuracy and stability of the LaunchPad were compared with a professional pulse generator BNC-505 by tracking a large number of droplet positions. The result shows that the LaunchPad is generally comparable with BNC-505. To validate the effectiveness of the whole setup, the droplet ejection and the droplet impact on the solid surface were quantitatively analyzed with the captured images. The experimental data extracted from the images in both
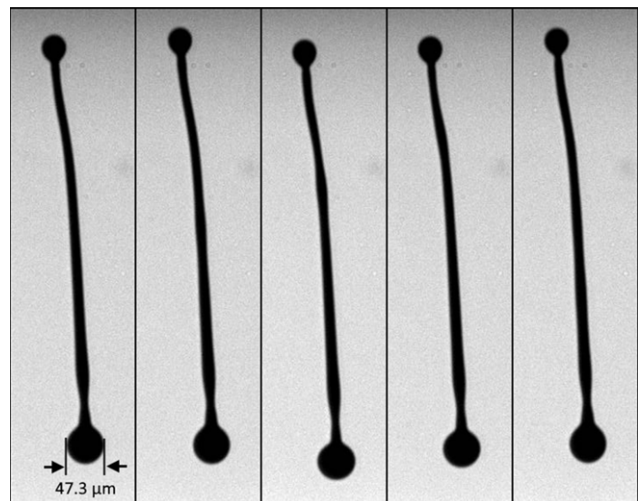

Figure 8. Images of droplets from a commercial inkjet captured by matching the interframe time to an integer multiple of the period between ejection events.

cases are in a good agreement with theoretical predictions. In the end, images of droplet ejected by the commercial cartridge are presented to demonstrate the performance of our imaging system.

APPENDIX. CODE FOR LAUNCHPAD

```
Int cam = 9;
Int inkjet = 10;
int strobe = 11;
int frequency = 10;    //Hz (Do not beyond 200 Hz)
int dwell_time = 10;    //µs
int delay_time  =  100;    // ms  (Actual delay time is
                           delay_time + dwell_time)
float period_delay = 1000/frequency;    //ms;
void setup()
{
 pinMode(cam, OUTPUT);
 pinMode(inkjet, OUTPUT);
 pinMode(strobe, OUTPUT);
}
void loop()
{
 digitalWrite(cam, HIGH);
 delayMicroseconds(dwell_time);
 digitalWrite(cam, LOW);
 delayMicroseconds(dwell_time);
 digitalWrite(inkjet, HIGH);
 delayMicroseconds(dwell_time);
 digitalWrite(inkjet, LOW);
 delayMicroseconds(delay_time);
 digitalWrite(strobe, HIGH);
 delayMicroseconds(dwell_time);
 digitalWrite(strobe, LOW);
 delay(period_delay);
}
```

REFERENCES

[1] I. M. Hutchings and G. Martin, *Inkjet Technology for Digital Fabrication* (Wiley, Chichester,West Sussex, United Kingdom, 2013), Vol. xii, p. 372.
[2] X. Kong, Y. Xi, P. LeDuff, E. Li, Y. Liu, L.-J. Cheng, G. L. Rorrer, H. Tan, and A. X. Wang, "Optofluidic sensing from inkjet-printed droplets: the enormous enhancement by evaporation-induced spontaneous flow on photonic crystal biosilica," Nanoscale **8**, 17285–17294 (2016).
[3] H. Wijshoff, "Drop dynamics in the inkjet printing process," Curr. Opin. Colloid Interface Sci. **62** (2018).
[4] M. Versluis, "High-speed imaging in fluids," Exp. Fluids **54** (2013).
[5] S. T. Thoroddsen, T. G. Etoh, and K. Takehara, " High-speed imaging of drops and bubbles," Annu. Rev. Fluid Mech. **40**, 257–285 (2008).
[6] G. D. Martin, S. D. Hoath, and I. M. Hutchings, "Inkjet printing-the physics of manipulating liquid jets and drops," J. Phys.: Conf. Ser. **105**, 012001 (2008).
[7] H. Dong, W. W. Carr, and J. F. Morris, "An experimental study of drop-on-demand drop formation," Phys. Fluids **18**, 072102 (2006).
[8] H. M. Dong, W. W. Carr, and J. F. Morris, "Visualization of drop-on-demand inkjet: Drop formation and deposition," Rev. Sci. Instrum. **77** (2006).
[9] I. M. Hutchings, G. D. Martin, and S. D. Hoath, "High speed imaging and analysis of jet and drop formation," J. Imaging Sci. Technol. **51**, 438–444 (2007).
[10] G. D. Martin, I. M. Hutchings, and S. D. Hoath, "Jet formation and late-stage ligament instability in drop-on-demand printing," *Proc. IS&T NIP27: Twenty-Seventh Int'l. Conf. on Digital Printing Technologies and Digital Fabrication* (IS&T, Springfield, 2006), Vol. 2006, pp. 95–98.
[11] Y. Kipman, P. Mehta, and K. Johnson, "Three methods of measuring velocity of drops in flight using jetxpert," *Proc. IS&T NIP & Digital Fabrication Conf.* (IS&T, Springfield, 2009), Vol. 2009, pp. 71–74.
[12] K. S. Kwon, "Speed measurement of ink droplet by using edge detection techniques," Measurement **42**, 44–50 (2009).
[13] K. S. Kwon, M. H. Jang, H. Y. Park, and H. S. Ko, "An inkjet vision measurement technique for high-frequency jetting," Rev. Sci. Instrum. **85** (2014).
[14] S. D. Hoath, "Standardization of inkjet drop speed measurement methods for printed electronics," *Proc. IS&T NIP & Digital Fabrication Conf.* (IS&T, Springfield, 2015), Vol. 2015, pp. 129–134.
[15] K. S. Kwon, H. S. Kim, and M. Choi, "Measurement of inkjet first-drop behavior using a high-speed camera," Rev. Sci. Instrum. **87** (2016).
[16] A. van der Bos, M. J. van der Meulen, T. Driessen, M. van den Berg, H. Reinten, H. Wijshoff, M. Versluis, and D. Lohse, "Velocity profile inside piezoacoustic Inkjet droplets in flight: comparison between experiment and numerical simulation," Phys. Rev. App. **1** (2014).
[17] Y. Son, C. Kim, D. H. Yang, and D. J. Alm, "Spreading of an inkjet droplet on a solid surface with a controlled contact angle at low weber and Reynolds numbers," Langmuir **24**, 2900–2907 (2008).
[18] W.-K. Hsiao, G. D. Martin, S. D. Hoath, and I. M. Hutchings, "Ink drop deposition and spreading in inkjet-based printed circuit board fabrication," *Proc. IS&T NIP & Digital Fabrication Conf.* (IS&T, Springfield, 2008), Vol. 2008, pp. 667–670.
[19] S. Jung and I. M. Hutchings, "The impact and spreading of a small liquid drop on a non-porous substrate over an extended time scale," Soft Matter **8**, 2686–2696 (2012).
[20] S. D. Hoath, W.-K. Hsiao, S. Jung, G. D. Martin, I. M. Hutchings, N. F. Morrison, and O. G. Harlen, "Drop speeds from drop-on-demand ink-jet print heads," J. Imaging Sci. Technol. **57**, 10503 (2013).
[21] J. Q. Chang, Y. X. Liu, and B. Huang, "Effects of dwell time of excitation waveform on meniscus movements for a tubular piezoelectric print-head: experiments and model," J. Micromech. Microeng. **27** (2017).
[22] D. Jang, D. Kim, and J. Moon, "Influence of fluid physical properties on ink-jet printability," Langmuir **25**, 2629–2635 (2009).
[23] S. D. Hoath, J. R. Castrejon-Pita, W. K. Hsiao, S. Jung, G. D. Martin, I. M. Hutchings, T. R. Tuladhar, D. C. Vadillo, S. A. Butler, M. R. Mackley, C. McIlroy, N. F. Morrison, O. G. Harlen, and H. N. G. Yow, "Jetting of complex fluids," J. Imaging Sci. Technol. **57** (2013).
[24] S. D. Hoath, I. M. Hutchings, G. D. Martin, T. R. Tuladhar, M. R. Mackley, and D. Vadillo, "Links between ink rheology, drop-on-demand jet formation, and printability," J. Imaging Sci. Technol. **53** (2009).
[25] A. van der Bos, A. Zijlstra, E. Gelderblom, and M. Versluis, "iLIF: illumination by Laser-Induced Fluorescence for single flash imaging on a nanoseconds timescale," Exp. Fluids **51**, 1283–1289 (2011).
[26] M. W. Davidson and M. Abramowitz, "Optical microscopy," *Encyclopedia of Imaging Science and Technology* (John Wiley & Sons, 2002).
[27] www.ti.com/tm4c123g-launchpad.
[28] J. Canny, "A computational approach to edge detection," *Readings in Computer Vision* (Royal Society of Chemistry, 1987), pp. 184–203.
[29] D. M. Harris, T. Liu, and J. W. Bush, "A low-cost, precise piezoelectric droplet-on-demand generator," Exp. Fluids **56**, 83 (2015).
[30] S. D. Hoath, "On international standards for in-flight measurements of inkjet drops," J. Imaging Sci. Technol. **62**, 010401 (2018).

31 G. D. Martin, W. C. Price, and I. M. Hutchings, "Measurement of inkjet drop volume—the role of image processing," J. Imaging Sci. Technol. **60**, 40401 (2016).

32 S. D. Hoath, S. Jung, and I. M. Hutchings, "A simple criterion for filament break-up in drop-on-demand inkjet printing," Phys. Fluids **25**, 021701 (2013).

33 L. Yang, B. K. Kazmierski, S. D. Hoath, S. Jung, W.-K. Hsiao, Y. Wang, A. Berson, O. Harlen, N. Kapur, and C. D. Bain, "Determination of dynamic surface tension and viscosity of non-Newtonian fluids from drop oscillations," Phys. Fluids **26**, 113103 (2014).

34 T. Lim, S. Han, J. Chung, J. T. Chung, S. Ko, and C. P. Grigoropoulos, "Experimental study on spreading and evaporation of inkjet printed pico-liter droplet on a heated substrate," Int. J. Heat Mass Transfer **52**, 431–441 (2009).

35 S. Schiaffino and A. A. Sonin, "Molten droplet deposition and solidification at low Weber numbers," Phys. Fluids **9**, 3172–3187 (1997).

36 I. S. Bayer and C. M. Megaridis, "Contact angle dynamics in droplets impacting on flat surfaces with different wetting characteristics," J. Fluid Mech. **558**, 415–449 (2006).